SEMICONDUCTORS

High ambipolar mobility in cubic boron arsenide revealed by transient reflectivity microscopy

Shuai Yue[1,2,3,4]†, Fei Tian[5,6]†, Xinyu Sui[1,4], Mohammadjavad Mohebinia[7], Xianxin Wu[1,4], Tian Tong[2], Zhiming Wang[3], Bo Wu[8], Qing Zhang[9], Zhifeng Ren[5]*, Jiming Bao[2,5,7]*, Xinfeng Liu[1,4]*

Semiconducting cubic boron arsenide (c-BAs) has been predicted to have carrier mobility of 1400 square centimeters per volt-second for electrons and 2100 square centimeters per volt-second for holes at room temperature. Using pump-probe transient reflectivity microscopy, we monitored the diffusion of photoexcited carriers in single-crystal c-BAs to obtain their mobility. With near-bandgap 600-nanometer pump pulses, we found a high ambipolar mobility of 1550 ± 120 square centimeters per volt-second, in good agreement with theoretical prediction. Additional experiments with 400-nanometer pumps on the same spot revealed a mobility of >3000 square centimeters per volt-second, which we attribute to hot electrons. The observation of high carrier mobility, in conjunction with high thermal conductivity, enables an enormous number of device applications for c-BAs in high-performance electronics and optoelectronics.

In 2018, the predicted high room-temperature thermal conductivity (κ) of cubic boron arsenide (c-BAs), >1300 W m^{-1} K^{-1}, was experimentally demonstrated (*1*–*3*). At about the same time, c-BAs was also predicted to have high carrier mobility values of 1400 cm^2 V^{-1} s^{-1} for electrons and 2100 cm^2 V^{-1} s^{-1} for holes (*4*). A higher hole mobility of >3000 cm^2 V^{-1} s^{-1} was later predicted under a small 1% strain (*5*). Such a high carrier mobility is due to a weak electron–phonon interaction and small effective mass (*4*–*7*). Like those predicting the thermal conductivity of c-BAs, these calculations were based on nondefective c-BAs with high crystal quality and a very low impurity level (*4*, *5*). The simultaneous high thermal conductivity and carrier mobility makes c-BAs a promising material for many applications in electronics and optoelectronics. Despite this potential, the high mobility has not been experimentally verified (*8*).

[1]Chinese Academy of Sciences (CAS) Key Laboratory of Standardization and Measurement for Nanotechnology, National Center for Nanoscience and Technology, Beijing 100190, China. [2]Department of Electrical and Computer Engineering and Texas Center for Superconductivity at the University of Houston (TcSUH), University of Houston, Houston, TX 77204, USA. [3]Institute of Fundamental and Frontier Sciences, University of Electronic Science and Technology of China, Chengdu, Sichuan 610054, China. [4]School of Nanoscience and Technology, University of Chinese Academy of Sciences, Beijing 100049, China. [5]Department of Physics and Texas Center for Superconductivity at the University of Houston (TcSUH), University of Houston, Houston, TX 77204, USA. [6]School of Materials Science and Engineering, Sun Yat-sen University, Guangzhou, Guangdong 510006, China. [7]Materials Science and Engineering Program, University of Houston, Houston, TX 77204, USA. [8]Guangdong Provincial Key Laboratory of Optical Information Materials and Technology and Institute of Electronic Paper Displays, South China Academy of Advanced Optoelectronics, South China Normal University, Guangzhou 510006, China. [9]School of Materials Science and Engineering, Peking University, Beijing 100871 China.
*Corresponding author. Email: zren@uh.edu (Z.R.); jbao@uh.edu (J.B.); liuxf@nanoctr.cn (X.L.)
†These authors contributed equally to this work.

In this study, using ultrafast spatial-temporal transient reflectivity microscopy, we observed an ambipolar mobility of ~1550 cm^2 V^{-1} s^{-1} and obtained a >3000 cm^2 V^{-1} s^{-1} mobility for photoexcited hot carriers. We used photoluminescence and Raman spectroscopy to probe the relative level of p-type doping and found that a high hole concentration will substantially reduce the ambipolar mobility.

We grew c-BAs single crystals using the same seeded chemical vapor transport technique reported previously (*3*, *9*). These crystals typically appear as slabs with (111) top and bottom surfaces. We used scanning electron microscopy to image a corner facet (111) of an as-grown c-BAs slab that we labeled sample 1 (Fig. 1A). This facet is one of the eight equivalent (111) surfaces, and we chose it for mobility measurement because of its relatively high quality, which can be seen from sharp (0.02°) characteristic peaks in the x-ray diffraction (XRD) pattern (Fig. 1B and inset), a narrow (0.6 cm^{-1}) longitudinal optical (LO) phonon peak at 700 cm^{-1} in the Raman spectrum (Fig. 1C and inset) (*1*, *2*), and the characteristic bandgap photoluminescence (PL) peak at 720 nm in the PL spectrum (Fig. 1D) (*10*), indicating high-quality crystal lattices, a low mass disorder (*11*), and a low defect density, respectively (*10*). PL mapping shown in the inset of Fig. 1D also indicates the uniform crystal quality on the (111) surface (*10*). We performed all measurements at room temperature and further characterized sample 1 and a second sample, labeled sample 2 (*12*) (fig. S1).

The Hall effect is the most common technique used to measure carrier mobility, but it requires four electrical contacts on a relatively large and uniform sample. To accommodate the requirements of mobility measurement in a small sample size or in inhomogeneous materials, ultrafast pump-probe techniques have been used to perform noncontact measurements with high spatial resolution (*13*–*17*). Because of our relatively thick samples, we used reflectivity rather than transmission. We focused a femtosecond pump pulse on c-BAs to photoexcite electrons and holes and monitored the diffusion of excited carriers in space and time with a time-delayed probe pulse defocused on a larger area (6 μm in diameter) (*12*) (Fig. 2A and fig. S2). We subsequently obtained an ambipolar mobility from the diffusion coefficient, D, through the Einstein relation, $D/k_BT = \mu/e$, where k_B is the Boltzmann constant, T is the temperature, μ is the mobility, and e is the elementary charge. Ambipolar mobility is given by $\mu_a = 2\mu_e\mu_h/(\mu_e + \mu_h)$, where μ_e and μ_h are the electron and hole mobility values, respectively. Because c-BAs has an electronic band structure similar to that of silicon, with an indirect bandgap in the range of 1.82 to 2.02 eV (*6*, *7*, *10*, *18*), we chose a 600-nm pump pulse and an 800-nm probe pulse to avoid the generation of hot carriers. Two-dimensional (2D) diffusion images in Fig. 2B show the expansion of carriers over 10 ps, and a representative time-resolved reflectivity as a function of the time delay between the pump and the probe is shown in Fig. 2C. A sudden negative differential reflectivity indicates a dominant electronic contribution, because reflectivity increases with lattice temperature (*12*, *19*) (fig. S3).

The spread of distributions in Fig. 2B reflects diffusion of photoexcited electrons and holes in space and time, and they can be well fit by Gaussian functions (Fig. 2D). The change in the variance σ^2 of carrier distributions is plotted in Fig. 2E. The linear increase in the variance with increasing time delay is a signature of diffusion, and the diffusion coefficient, D, can be calculated from the slope using the equation $\sigma_t^2 = \sigma_0^2 + \alpha Dt$, where α is a constant depending on the dimensions of the system and detection configuration (*15*). We chose an α of 2 for our experiment because of the much larger laser penetration (excitation) depth (60 μm at 600 nm) compared with the thin top layer sampled by the probe beam [20 nm at 800 nm, given by $\lambda/4\pi n$ (*13*, *15*–*17*, *19*), where n is the refractive index of c-BAs (*18*)]. From the slope of the curve shown in Fig. 2E and the Einstein relation, $D/k_BT = \mu/e$, we obtained an ambipolar diffusion coefficient of ~39 cm^2 s^{-1} and an ambipolar mobility of 1550 ± 120 cm^2 V^{-1} s^{-1}, close to the predicted value (*4*).

Given that the properties of c-BAs are not uniform even within a single crystal, especially in the direction perpendicular to (111) surfaces (*3*, *10*), we tested a cross-sectional surface of a relatively thin (30-μm-thick) crystal labeled sample 2 (*12*) (fig. S1). An optical image of the sample 2 sidewall is shown in the inset of Fig. 3A. We obtained PL spectra from several spots at different distances from the edge (Fig.

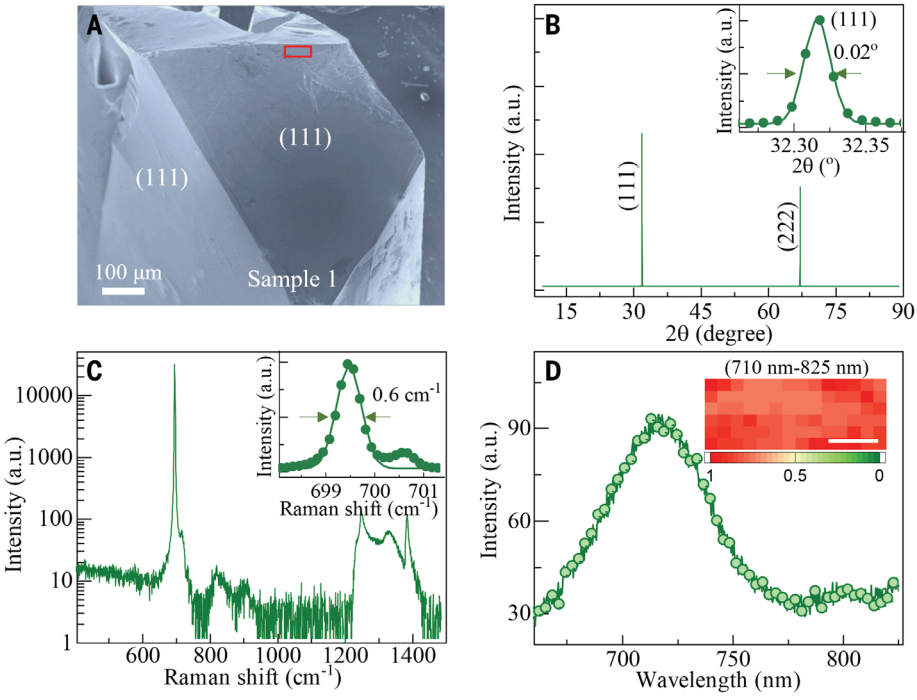

Fig. 1. Characterizations of a c-BAs single crystal (sample 1) on a corner (111) facet. (**A**) Scanning electron microscopy image. Scale bar: 100 μm. (**B**) X-ray diffraction pattern. (Inset) Magnified view of the (111) peak. (**C**) Raman spectrum excited by a 532-nm laser. (Inset) High-resolution spectrum of the LO phonon. (**D**) Photoluminescence spectrum excited by a 593-nm laser. (Inset) photoluminescence mapping from the region marked by a red rectangle in (A). Scale bar: 10 μm. a.u., arbitrary units.

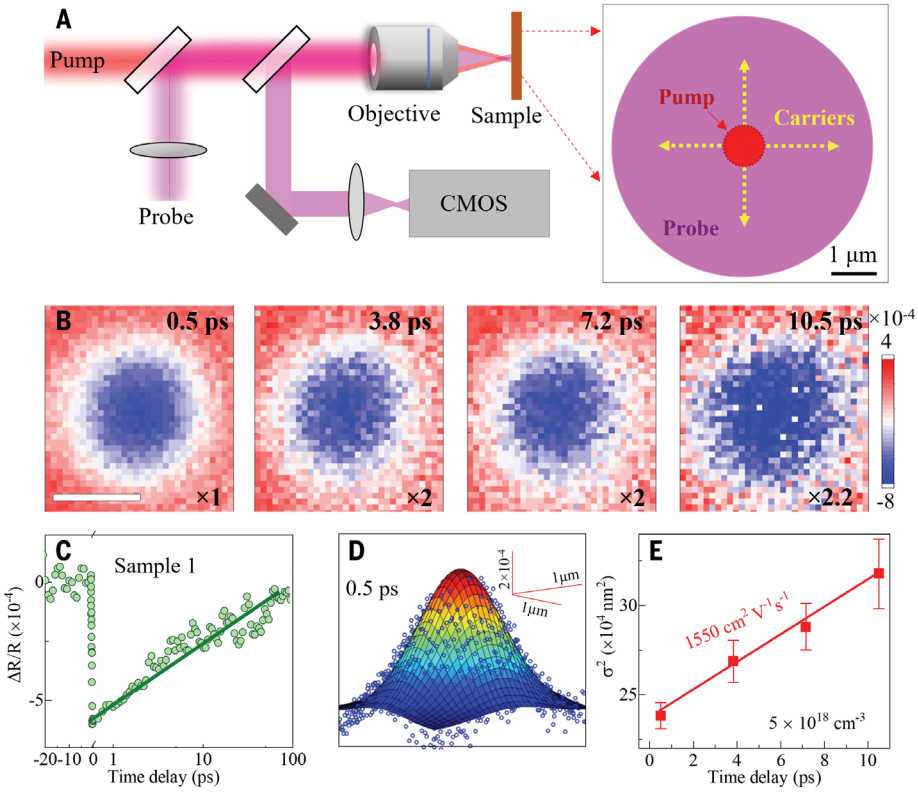

Fig. 2. Pump-probe transient reflectivity microscopy, carrier dynamics, and diffusion in sample 1. (**A**) Schematic illustration of the experimental setup. CMOS, complementary metal-oxide semiconductor. (**B**) Evolution of a 2D transient reflectivity microscopy image from a spot on sample 1. Scale bar: 1 μm. (**C**) Typical transient reflectivity dynamics (photoexcited carrier density of 5×10^{18} cm^{-3}). (**D**) Spatial profile (dots) and Gaussian fit at 0.5 ps time delay from (B) (fig. S4). (**E**) Evolution of variance of Gaussian distributions extracted from Gaussian fitting in (D). The corresponding mobility is included.

3A). The PL intensity increases with decreasing distance from the edge and exhibits a noticeable jump upon reaching the (111) surface, which agrees with our previous finding of a drastic change in PL from one surface to the opposite surface of a single crystal slab (*10*). Corresponding Raman spectra from the same locations are shown in Fig. 3B and its inset. Similar to the PL results, the Raman spectrum of the (111) surface differs substantially from those of the sidewall. We chose a spot ~11 μm from the edge (Fig. 3A, dashed circle in inset) and used three pump fluences to create different carrier densities, the reflectivity distributions of which are shown in Fig. 3, C and D, and fig. S6 (*12*). We plotted the evolution of the variances and obtained an ambipolar mobility of ~1300 cm^2 V^{-1} s^{-1} (Fig. 3E), indicating the negligible effect of carrier density on the mobility of sample 2 owing to nonlinear effects such as Auger recombination.

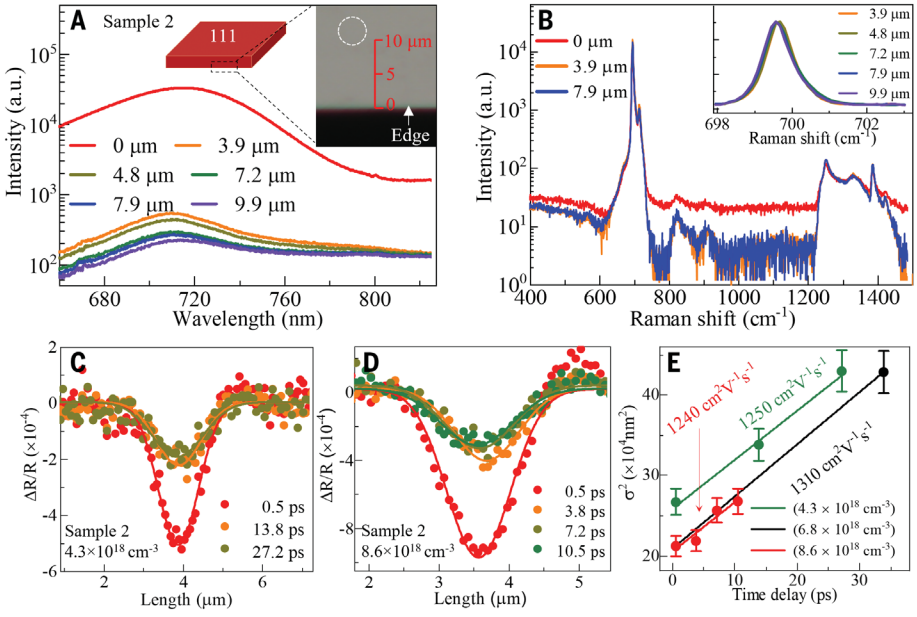

Fig. 3. Carrier diffusion on a cross-sectional surface of sample 2. (**A**) PL spectra of six locations on a cross-sectional surface with increasing distance from the edge. PL of the spot at 0 μm was taken from the (111) surface around the edge. (Inset) Optical image of the sidewall. Dashed circle indicates location for pump-probe measurements in (C) to (E). (**B**) Raman spectra of three of the six locations shown in (A). (Inset) Magnified view of the phonon line in the spectra of the five sidewall locations. (**C** and **D**) Spatial profiles (dots) and Gaussian fits (curves) of photoexcited carriers at initial concentrations of 4.3 × 10^{18} cm^{-3} and 8.6 × 10^{18} cm^{-3}, respectively, from a location indicated by the dashed circle in (A). (**E**) Variance and ambipolar mobility values from (C), (D), and fig. S6.

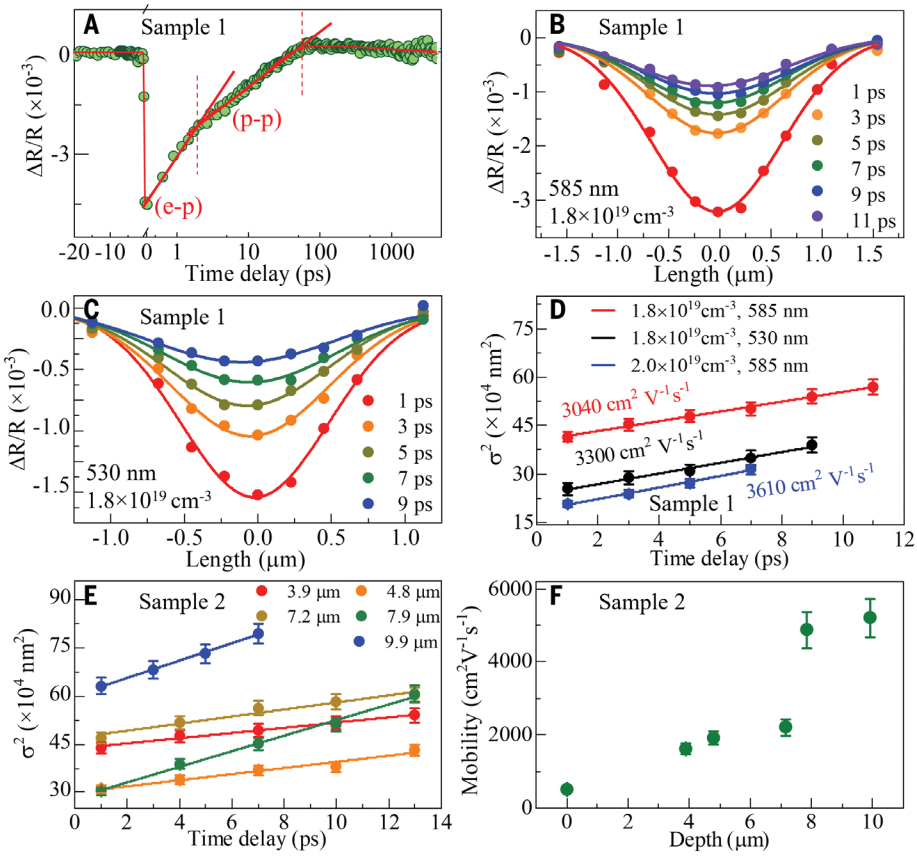

Fig. 4. Transient reflectivity microscopy and carrier diffusion measured using a 400-nm pump and a 585- or 530-nm probe. (**A**) Representative pump-probe transient reflectivity curve from sample 1. The probe wavelength is 585 nm. (**B** and **C**) Spatial profiles (dots) and Gaussian fits (curves) of transient reflectivity from a spot in sample 1 measured using 585- and 530-nm probes, respectively. (**D**) Evolution of the variances of carrier density distributions and carrier mobility from (B), (C), and fig. S10. (**E** and **F**) Variance and ambipolar mobility results, respectively, for sample 2 at six locations corresponding to those shown in Fig. 3, A and B.

The high carrier mobility of c-BAs is enabled by its distinctive weak electron–phonon interaction and its phonon–phonon scattering, which should also enable the generation of high-mobility hot carriers (*20*). To prove this, we used a 400-nm pulse as a pump and selected a particular band (585 or 530 nm) with an optical filter from a white light continuum beam as a probe pulse (*12*) (fig. S7). A typical transient reflectivity curve of a probe (585 nm) from sample 1 is shown in Fig. 4A. In contrast to the single exponential decay previously observed when excited by a 600-nm pump (Fig. 2C), the dynamics of photoexcited carriers excited by the 400-nm pump consist of three exponential decays: a fast exponential decay with a ~1-ps lifetime, a slow decay of ~20 ps, and an even slower decay on the order of 1 ns (*21*). These decays correspond to rapid relaxation of high-energy photoexcited carriers, further relaxation of carriers to the conduction and valence band edges, and a combination of lattice heating and recombination and trapping of electrons

and holes at the band edges, respectively (*20*, *21*), in good agreement with the theoretical prediction (*20*). To obtain the diffusion coefficient of the carriers in sample 1, we used a simpler method by varying the relative displacement between focused pump and probe beams along one direction (*12*) (figs. S7 and S8). We plotted the resulting spatial profiles of the reflectivity after 1 ps for probe wavelengths of 530 and 585 nm (Fig. 4, B and C) (*12*) and obtained an ambipolar diffusion coefficient of 80 $cm^2\ s^{-1}$ and an ambipolar mobility of ~3200 $cm^2\ V^{-1}\ s^{-1}$ (Fig. 4D). Mobility of ~3600 $cm^2\ V^{-1}\ s^{-1}$ was obtained from the same spot as that shown in Fig. 2 for sample 1. These values are much larger than the predicted ambipolar mobility of 1680 $cm^2\ V^{-1}\ s^{-1}$ (*4*).

Using the same 400-nm pump, we also measured the ambipolar mobility of sample 2 at six locations corresponding to those shown in Fig. 3, A and B. The evolution of variance of carrier distribution at these spots is shown in Fig. 4, E and F, and fig. S11. The differences in the initial values of the variances at 1 ps are due to the different spot sizes of the pump and probe beams in each measurement. The mobility clearly changes drastically across the sidewall, with the highest mobility (5200 ± 600 $cm^2\ V^{-1}\ s^{-1}$) observed at a depth of 9.9 μm. Although local strain could result in such prominent carrier mobility enhancement (*5*), we did not see any noticeable Raman shift among these locations (Fig. 3B). We thus attribute the high ambipolar mobility to photoexcited hot carriers, which exhibit high carrier diffusion coefficient and mobility values (*20*, *22*–*24*).

The position-dependent mobility on the sidewall of sample 2 reveals that p-type doping in c-BAs can substantially reduce its mobility. Heavy p-type doping on the (111) surface can be seen from the Fano line shape of the LO phonon at 700 cm^{-1} and the higher background level around 1000 cm^{-1} (Fig. 3B) (*2*, *8*). This gradually increased doping level toward the (111) surface is further supported by the corresponding increased PL intensity (*10*, *25*). P-type doping will result in reduced carrier mobility owing to the presence of ionized dopants (these dopants are already activated) and a lower electron mobility than hole mobility, because minority carriers will dominate the carrier dynamics. The latter is supported by our observation of a higher ambipolar mobility in p-type silicon than in undoped silicon (*12*) (figs. S12 and S13). Clearly, the enhanced PL intensity observed in the c-BAs samples in the current study indicates that p-type doping has only introduced shallow acceptors rather than nonradiative deep levels (*10*, *25*). Because hot carriers can also be generated by electrical injection and low-intensity light, both hot carriers and fully relaxed carriers can be used for high-speed optoelectronic devices and high-efficiency solar cells in conjunction with the high mobility of the band-edge carriers.

REFERENCES AND NOTES

1. J. S. Kang, M. Li, H. Wu, H. Nguyen, Y. Hu, *Science* **361**, 575–578 (2018).
2. S. Li *et al*., *Science* **361**, 579–581 (2018).
3. F. Tian *et al*., *Science* **361**, 582–585 (2018).
4. T.-H. Liu *et al*., *Phys. Rev. B* **98**, 081203 (2018).
5. K. Bushick, S. Chae, Z. Deng, J. T. Heron, E. Kioupakis, *NPJ Comput. Mater.* **6**, 3 (2020).
6. J. L. Lyons *et al*., *Appl. Phys. Lett.* **113**, 251902 (2018).
7. K. Bushick, K. Mengle, N. Sanders, E. Kioupakis, *Appl. Phys. Lett.* **114**, 022101 (2019).
8. X. Chen *et al*., *Chem. Mater.* **33**, 6974–6982 (2021).
9. F. Tian *et al*., *Appl. Phys. Lett.* **112**, 031903 (2018).
10. S. Yue *et al*., *Mater. Today Phys.* **13**, 100194 (2020).
11. A. Rai, S. Li, H. L. Wu, B. Lv, D. G. Cahill, *Phys. Rev. Mater.* **5**, 013603 (2021).
12. See supplementary materials.
13. Y. Wan *et al*., *Nat. Chem.* **7**, 785–792 (2015).
14. M. M. Gabriel *et al*., *Nano Lett.* **13**, 1336–1340 (2013).
15. N. S. Ginsberg, W. A. Tisdale, *Annu. Rev. Phys. Chem.* **71**, 1–30 (2020).
16. R. Wang *et al*., *Phys. Rev. B* **86**, 045406 (2012).
17. L. Yuan *et al*., *Nat. Mater.* **19**, 617–623 (2020).
18. B. Song *et al*., *Appl. Phys. Lett.* **116**, 141903 (2020).
19. A. J. Sabbah, D. M. Riffe, *Phys. Rev. B* **66**, 165217 (2002).
20. S. Sadasivam, M. K. Y. Chan, P. Darancet, *Phys. Rev. Lett.* **119**, 136602 (2017).
21. Z. Y. Tian *et al*., *Phys. Rev. B* **105**, 174306 (2022).
22. A. Block *et al*., *Sci. Adv.* **5**, eaav8965 (2019).
23. B. A. Ruzicka *et al*., *Phys. Rev. B* **82**, 195414 (2010).
24. E. Najafi, V. Ivanov, A. Zewail, M. Bernardi, *Nat. Commun.* **8**, 15177 (2017).
25. S. Y. Lim *et al*., *IEEE J. Photovolt.* **3**, 649–655 (2013).

ACKNOWLEDGMENTS

We thank X. Bo and L. Yang for help with high-resolution Raman and XRD measurements. We thank J. Ding and X. Qiu for help with the AFM measurement. We thank J. Zhao for helpful discussion. **Funding:** The work performed in China was supported by the Strategic Priority Research Program of the Chinese Academy of Sciences (XDB36000000); the Ministry of Science and Technology (2017YFA0205004); the National Natural Science Foundation of China (22173025, 22073022, 11874130, and 52172171); the CAS Instrument Development Project (Y950291); and the DNL Cooperation Fund, CAS (DNL202016). The work performed at the University of Houston (UH) is supported by the Office of Naval Research under Multidisciplinary University Research Initiative grant N00014-16-1-2436, the Welch Foundation (E-1728), and a UH Small Equipment Grant (000182016). **Author contributions:** X.L., J.B., and Z.R. conceived of the project. S.Y. performed the Raman, PL, transient reflectivity, and transient reflectivity microscopy experiments. F.T. grew the crystal samples. X.S. and S.Y. built the transient reflectivity setup. S.Y. built the transient reflectivity microscopy setup. M.M. performed the carrier diffusion and laser heating simulation. X.W. performed the high-resolution Raman experiment. T.T. performed the temperature-dependent reflectivity experiment. B.W. performed the carrier diffusion theoretical analysis. J.B., S.Y., Z.R., X.L., Z.W., and Q.Z. wrote the paper. All authors contributed to the discussion of the results and writing of the manuscript. **Competing interests:** The authors declare that they have no competing interests. The c-BAs crystals were grown by the method disclosed in US patent publication 20210269318 and a new patent filing on high mobility. **Data and materials availability:** All data are available in the main text or the supplementary materials.

SUPPLEMENTARY MATERIALS

science.org/doi/10.1126/science.abn4727
Materials and Methods
Supplementary Text
Figs. S1 to S13
References (*26*, *27*)

Submitted 1 December 2021; accepted 16 June 2022
10.1126/science.abn4727

Science

High ambipolar mobility in cubic boron arsenide revealed by transient reflectivity microscopy

Shuai YueFei TianXinyu SuiMohammadjavad MohebiniaXianxin WuTian TongZhiming WangBo WuQing ZhangZhifeng RenJiming BaoXinfeng Liu

Science, 377 (6604), • DOI: 10.1126/science.abn4727

Swift carriers

Boron arsenide is a semiconductor with several interesting properties, including a high thermal conductivity. Theoretical calculations also suggest that it has high ambipolar mobility, a measure of the mobility of electrons and holes. Yue *et al*. and Shin *et al*. used different types of measurements to observe a high ambipolar mobility in very pure cubic boron arsenide. Shin *et al*. were able to simultaneously measure the high thermal and electrical transport properties in the same place in their samples. Yue *et al*. found even higher ambipolar mobility than the theoretical estimates at a few locations. Boron arsenide's combination of transport properties could make it an attractive semiconductor for various applications. —BG